INTERNATIONAL JOURNAL FOR NUMERICAL METHODS IN ENGINEERING, VOL. 37, 2631–2655 (1994)

ADAPTIVE FINITE ELEMENT ANALYSIS OF GEOMETRICALLY NON-LINEAR PLATES AND SHELLS, ESPECIALLY BUCKLING

E. STEIN, B. SEIFERT AND S. OHNIMUS

Institute of Structural and Computational Mechanics (IBNM) University of Hannover, Germany

C. CARSTENSEN

Institute of Applied Mathematics, University of Hannover, Germany

SUMMARY

Based on both moderate and finite rotation bending theories of thin elastic shells including shear deformation, adaptive non-linear static finite element analysis is treated within a displacement approach and *h*-adaptivity. The *a posteriori* error indicator given by Rheinboldt, gained by linearization, is investigated in order to decide whether the deformations influence the indicator explicitely and how parameter dependent problems (like the Reissner–Mindlin model) behave in the process of adaptation. In order to achieve overall consistency, dimensional adaptivity (to 3-D elasticity) is implemented within disturbed subdomains, especially at supports.

Results are that Rheinboldt's error indicator is valid under certain restrictions but not directly at bifurcation points and that robustness is not improved by adaptation.

Nested quadrilateral finite elements are used for studying pre- and post-buckling states of plates and shells.

INTRODUCTION

Moderate and finite rotation theories[1–3] are available including the finite element analysis, especially the treatment of shear locking problems. The shell model used in this paper is based on geometrically non-linear Reissner–Mindlin kinematics where the finite element formulation may be derived from first Piola–Kirchhoff, Biot or second Piola–Kirchhoff stress resultants alternatively. Inextensibility in the thickness direction is assumed as well as the restriction of small strains which results after elimination of drilling degrees of freedom in a five-parameter shell model. The description of finite rotations of the shell normal is expressed in terms of a scew-symmetric tensor.

In the frame of *h*-adaptivity, a general error analysis for geometrically non-linear problems is not available up to now. Several papers from Rheinboldt[4] and the recent work by Verführt[5] try to justify the use of the well known linear Babuska–Miller[1,2] error-estimator even for geometrically non-linear problems. The presented arguments in Reference 4 are based on the linearized non-linear problem, but the accuracy of the underlying metric in the non-linear continuum-mechanical settings are not discussed. In this paper more general conditions of this proof are taken into account and robustness features depending of the chosen shell model are investigated. Furthermore, the validity of the results for two important situations, bifurcation problems and

CCC 0029–5981/94/152631–25$9.00

Received 6 October 1993

locking phenomena, which are of great interest in finite-element applications, are discussed. A frame for efficient numerical implementation is given too.

Following geometrical non-linear load displacement paths a suitable refinement strategy is presented including bifurcation problems. Such adaptive methods for detecting local and global buckling need consistent and stable modelling in conjunction with reliable numerical approximations. Therefore, dimensional adaptivity is taken into account to solve these shortcomings, mainly at supports.

Three numerical examples are presented in order to show the effectivity of the error indicators, to give a deeper insight into the investigated shell problems and illustrate the proposed solutions strategies.

A THIN SHELL ELEMENT FOR SMALL ELASTIC STRAINS AND FINITE ROTATIONS

In this section we discuss a five-parameter finite element formulation applicable to structural problems with finite rotations and small strains. A displacement approach is used which includes shear deformation and therefore belongs to non-linear Reissner–Mindlin type theories.[21] The kinematics for the finite element formulation are derived from the description of the movement of an orthonormal cartesian frame during deformation, identical with the initial normal vector and the tangents in the undeformed state. Since shear deformation is included, the rotated director is not normal to the deformed middle surface, and therefore the rotated base vectors do not remain tangents to the deformed surface. Modern approaches to this treatment of shells not using the traditional strain measures in convected co-ordinate systems were given by Gruttmann et al.[2] and Simo[3] amongst others. Only two independent rotational degrees of freedom are used to describe the rotations of the cartesian frame, and therefore arbitrary but smooth surfaces can be modelled with C^0 continuous shape functions. The use of drilling degrees of freedom affects zero energy modes, especially within the treatment of stability problems, see also Reference 3. In order to overcome the problems associated with shear locking we choose the assumed strain element suggested by Bathe and Dvorkin.[6] For the sake of convenience we restrict ourselves in this paper to the St. Venant–Kirchhoff hyperelastic material law for small strains.

Kinematics of the shell

The usual kinematical setting describes the position of an arbitrary point in the shell space where $\mathbf{x}$ denotes its position vector in the current configuration, see Figure 1.

$$\mathbf{x} = \mathbf{x}_0 + s_3\mathbf{a}_3, \quad -\frac{h}{2} \leqslant s_3 \leqslant \frac{h}{2} \tag{1}$$

Here

$$\mathbf{x}_0 = \mathbf{X}_0 + \mathbf{u} = (X_{0i} + u_i)\mathbf{e}_i \tag{2}$$

describes the translation of the shell middle surface from its initial into the current configuration whereas s_3 is the co-ordinate in the thickness direction and $\mathbf{a}_3$ the shell director in the current configuration.

Furthermore, we introduce an orthonormal co-ordinate system $\mathbf{t}_i$ in the reference configuration where the vectors $\mathbf{t}_1$ and $\mathbf{t}_2$ are tangents to the shell middle surface, and s_1 and s_2 are the associated co-ordinates. An additional orthonormal basis is constructed in the current configura-

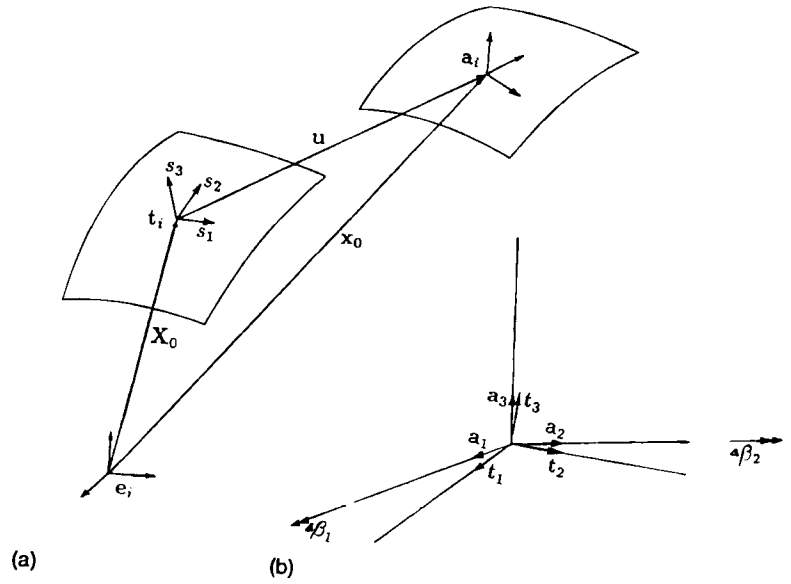

Figure 1. (a) Reference and current configuration of a shell, (b) finite rotations

tion of the shell, and the following relations between the two different bases hold.

$$\mathbf{t}_i(s_\alpha) = \mathbf{R}_0(s_\alpha)\mathbf{e}_i, \quad \mathbf{a}_i(s_\alpha) = \mathbf{R}(s_\alpha)\mathbf{t}_i, \quad \alpha = 1, 2 \tag{3}$$

Since the two matrices $\mathbf{R}_0$ and $\mathbf{R}$ describe an orthogonal transformation, the Euclidean norm of the director vector $\mathbf{a}_3$ remains unchanged during deformation, and extensibility in thickness direction is therefore excluded. The following expressions for the derivatives of the base vectors are necessary for subsequent development:

$$\frac{\partial \mathbf{t}_i(s_\alpha)}{\partial s_\alpha} = \boldsymbol{\Omega}_{0\alpha}\mathbf{t}_i, \quad \frac{\partial \mathbf{a}_i(s_\alpha)}{\partial s_\alpha} = (\boldsymbol{\Omega}_\alpha + \mathbf{R}\boldsymbol{\Omega}_{0\alpha}\mathbf{R}^{\mathrm{T}})\mathbf{a}_i \tag{4}$$

The scew-symmetric tensors $\boldsymbol{\Omega}_{0\alpha}$ and $\boldsymbol{\Omega}_\alpha$

$$\boldsymbol{\Omega}_{0\alpha} = \frac{\partial \mathbf{R}_0(s_\alpha)}{\partial s_\alpha}\mathbf{R}_0^{\mathrm{T}}, \quad \boldsymbol{\Omega}_\alpha = \frac{\partial \mathbf{R}(s_\alpha)}{\partial s_\alpha}\mathbf{R}^{\mathrm{T}} \tag{5}$$

are related to associated axial vectors $\boldsymbol{\omega}_{0\alpha}$ and $\boldsymbol{\omega}_\alpha$ which allow to reformulate the above equations

$$\frac{\partial \mathbf{t}_i(s_\alpha)}{\partial s_\alpha} = \boldsymbol{\omega}_{0\alpha} \times \mathbf{t}_i, \quad \frac{\partial \mathbf{a}_i(s_\alpha)}{\partial s_\alpha} = (\boldsymbol{\omega}_\alpha + \mathbf{R}\boldsymbol{\omega}_{0\alpha}) \times \mathbf{a}_i \tag{6}$$

Variational formulation

We define stress resultants and stress couple resultants by integration of the stress vectors $\mathbf{t}_\alpha$ over the shell thickness

$$\mathbf{n}_\alpha = \int_{-h/2}^{h/2} \mathbf{t}_\alpha \, ds_3, \quad \mathbf{m}_\alpha = \int_{-h/2}^{h/2} (\mathbf{x} - \mathbf{x}_0)\mathbf{t}_\alpha \, ds_3 \tag{7}$$

The stress vectors $\mathbf{t}_\alpha$ of the current configuration are measured with respect to the undeformed cross-section, i.e. they are derived from $\mathbf{P} = \mathbf{t}_i \otimes \mathbf{e}_i$. No drilling moments occur within the chosen settings, $M_{\alpha 3} = (\mathbf{m}_\alpha \times \mathbf{a}_3)\cdot \mathbf{a}_3 = 0$. The derivation of the variational form starts from static field equations for the 3-D theory expressed in terms of the first Piola–Kirchhoff stress tensor in the reference configuration

$$\operatorname{div} \mathbf{P} + \rho \mathbf{b}_0 = 0, \quad \mathbf{F} \times \mathbf{P} = \mathbf{0}, \quad \mathbf{F} = \operatorname{Grad} \mathbf{x}(\mathbf{X}) \tag{8}$$

These equations are integrated and yield the equilibrium conditions for the stress- and stress-couple resultants as well as the associated boundary conditions

$$\frac{\partial \mathbf{n}_1}{\partial s_1} + \frac{\partial \mathbf{n}_2}{\partial s_2} + \tilde{\mathbf{q}} = \mathbf{0} \tag{9}$$

$$\frac{\partial \mathbf{m}_1}{\partial s_1} + \frac{\partial \mathbf{m}_2}{\partial s_2} + \frac{\partial \mathbf{x}_0}{\partial s_1} \times \mathbf{n}_1 + \frac{\partial \mathbf{x}_0}{\partial s_2} \times \mathbf{n}_2 + \tilde{\mathbf{m}} = \mathbf{0} \tag{10}$$

Following Gruttmann *et al.*[2] we proceed with standard variational calculus and multiply the above Euler–Lagrange equations with statically admissible variations. After application of the divergence theorem the final result for the static weak formulation with first Piola–Kirchhoff stress resultants is

$$\delta W = \int_\Omega (\mathbf{n}_\alpha \delta \hat{\boldsymbol{\varepsilon}}_\alpha + \mathbf{m}_\alpha \delta \hat{\boldsymbol{\kappa}}_\alpha)\, \mathrm{d}\Omega \tag{11}$$

where the associated virtual strain measures are

$$\delta \hat{\boldsymbol{\varepsilon}}_\alpha = \delta \mathbf{x}_{0,\alpha} - \delta \mathbf{w} \times \mathbf{x}_{0,\alpha}, \quad \delta \hat{\boldsymbol{\kappa}}_\alpha = \delta \mathbf{x}_{0,\alpha} - \delta \mathbf{w} \times (\boldsymbol{\omega}_\alpha + \mathbf{R}\boldsymbol{\omega}_{0\alpha}), \quad \delta \mathbf{a}_i := \delta \mathbf{w} \times \mathbf{a}_i \tag{12}$$

An equivalent expression for the internal virtual work is given in terms of Biot stress resultants $\mathbf{N}_\alpha = \mathbf{R}_0^{\mathrm{T}} \mathbf{R}^{\mathrm{T}} \mathbf{m}_\alpha$, $\mathbf{M}_\alpha = \mathbf{R}_0^{\mathrm{T}} \mathbf{R}^{\mathrm{T}} \mathbf{n}_\alpha$ and work conjugated strain measures connected with the right stretch tensor $\mathbf{U}$. We derive

$$\delta W = \int_\Omega (\mathbf{N}_\alpha \delta \boldsymbol{\varepsilon}_\alpha + \mathbf{M}_\alpha \delta \boldsymbol{\kappa}_\alpha)\, \mathrm{d}\Omega \tag{13}$$

and get the variational strain measures

$$\delta \boldsymbol{\varepsilon}_\alpha = \mathbf{R}_0^{\mathrm{T}} \mathbf{R}^{\mathrm{T}} \delta \hat{\boldsymbol{\varepsilon}}_\alpha = \delta (\mathbf{R}_0^{\mathrm{T}} \mathbf{R}^{\mathrm{T}} \mathbf{x}_{0,\alpha}), \quad \delta \boldsymbol{\kappa}_\alpha = \mathbf{R}_0^{\mathrm{T}} \mathbf{R}^{\mathrm{T}} \delta \hat{\boldsymbol{\kappa}}_\alpha = \delta (\mathbf{R}_0^{\mathrm{T}} \mathbf{R}^{\mathrm{T}} \boldsymbol{\omega}_\alpha) \tag{14}$$

where initial curvatures $\boldsymbol{\omega}_{0\alpha}$ are neglected. Membrane strain measures and related work conjugated membrane stress resultants connected with the first Piola–Kirchhoff tensor are not *a priori* symmetric. The same feature is shown by strain measures and stress resultants connected with the right stretch tensor $\mathbf{U}$ and the Biot stress tensor. Following Wriggers and Gruttmann[7] and making use of a polar decomposition,

$$a_{\alpha i} = (\mathbf{R}_0^{\mathrm{T}} \mathbf{R}^{\mathrm{T}} \mathbf{x}_{0,\alpha}) \cdot \mathbf{e}_i = \mathbf{x}_{0,\alpha} \cdot \mathbf{a}_i \quad a_{\alpha\beta} = \Lambda_{\alpha\gamma} \tilde{a}_{\gamma\beta}, \quad \tilde{a}_{\alpha\beta} = \tilde{a}_{\beta\alpha} \tag{15}$$

symmetric membrane strains are obtained as

$$\tilde{\varepsilon}_{\alpha\beta} = \tilde{\alpha}_{\alpha\beta} - \delta_{\alpha\beta} \tag{16}$$

Using the Green Lagrangian strain measure of the 3-D problem ($\mathbf{E} = (1/2)(\mathbf{F}^{\mathrm{T}}\mathbf{F} - \mathbf{1})$), we get the membrane strains

$$\varepsilon_{\alpha\beta} = \tfrac{1}{2}(\mathbf{x}_{0,\alpha} \cdot \mathbf{x}_{0,\beta} - \mathbf{X}_{0,\alpha} \cdot \mathbf{X}_{0,\beta}) \tag{17}$$

the shear strains

$$\gamma_\alpha = \mathbf{x}_{0,\alpha} \cdot \mathbf{a}_3 - \mathbf{X}_{0,\alpha} \cdot \mathbf{t}_3$$

and the elastic curvatures

$$\kappa_{\alpha\beta} = \mathbf{x}_{0,\alpha} \cdot \mathbf{a}_{3,\beta} - \mathbf{X}_{0,\alpha} \cdot \mathbf{t}_{3,\beta}$$

The related stress resultants and stress couple resultants $\tilde{N}_{\alpha\beta}$, $\tilde{M}_{\alpha\beta}$ and $\tilde{Q}_\alpha$ are based on the second Piola–Kirchhoff stress tensor. The virtual work of the internal forces then reads

$$\delta W = \int_\Omega (\tilde{N}_{\alpha\beta}\delta\varepsilon_{\alpha\beta} + \tilde{M}_{\alpha\beta}\delta\kappa_{\alpha\beta} + \tilde{Q}_\alpha\delta\gamma_\alpha)\,\mathrm{d}\Omega \tag{18}$$

The straightforward derivation of second Piola–Kirchhoff stress resultants from Biot stress resultants is shown in Reference 8.

Geometry interpolation and finite element discretization

In this section the finite element formulation for the theory described above is summarized. Since the formulation in the previous section involves only axial vectors and the rotation tensor, a specified representation of the rotations does not influence the general equations. For instance, quaternions or angles with a certain combination of rotations about follower axes (e.g. Eulerian angles) can be useful. The finite element formulation has to be done carefully because singularities may occur in the solutions.

The chosen unknowns for the rotations are the components of the incremental axial pseudo-vector $\Delta\mathbf{w}^i$. The associated skew-symmetric matrix $\Delta\boldsymbol{\Omega}^i$ results from a linearization of the incremental rotation tensor, i.e. a Taylor expansion of the tensor $\Delta\mathbf{R}^i$. This parametrization is supposed to be singularity free. The update of the whole rotation tensor $\mathbf{R}^i$ within each step of the Newton iteration is computed exactly with the incremental tensor $\Delta\mathbf{R}^i$.[3,9]

An isoparametric C^0 continuous approach is used, and five nodal values (subscript k) are interpolated with bilinear interpolation functions (N_k). A superscript i denotes a single step of the Newton iteration. The incremental nodal displacement vector is defined as

$$\Delta\mathbf{V}_k^{i\mathrm{T}} = [\Delta v_{1k}^i, \Delta v_{2k}^i, \Delta v_{3k}^i, \Delta\beta_{1k}^i, \Delta\beta_{2k}^i] = [\Delta\mathbf{u}_k^{i\mathrm{T}}, \Delta\boldsymbol{\beta}_k^{i\mathrm{T}}]$$

with

$$\Delta\mathbf{x}^i = \sum_k N_k \Delta\mathbf{x}_k^i, \quad \Delta\mathbf{u}^i = \sum_k N_k \Delta\mathbf{u}_k^i, \quad \Delta\mathbf{w}^i = \sum_k N_k \Delta\mathbf{w}_k^i \tag{19}$$

Two independent local rotation angles $\Delta\boldsymbol{\beta}^i$ are transformed into the three global rotation angles $\Delta\mathbf{w}^i$ with the matrix $\boldsymbol{\Lambda}$,

$$\Delta\mathbf{w}^i = \boldsymbol{\Lambda}\,\Delta\boldsymbol{\beta}^i, \quad \boldsymbol{\Lambda} = [\mathbf{a}_1|\mathbf{a}_2] \tag{20}$$

At nodal points the update of the displacement field is obtained additively,

$$\mathbf{u}^{i+1} = \Delta\mathbf{u}^i + \mathbf{u}^i \tag{21}$$

whereas the rotation field needs a multiplicative update starting from the initial position of the cartesian frame

$$\mathbf{R}^0 = [\mathbf{t}_1|\mathbf{t}_2|\mathbf{t}_3] \tag{22}$$

which leads to

$$\mathbf{R}^{i+1} = \Delta\mathbf{R}^i\mathbf{R}^i, \quad \mathbf{R}^i = [\mathbf{a}_1|\mathbf{a}_2|\mathbf{a}_3]^i \tag{23}$$

From equations (20) and (23) the following expression for the Taylor expansion of $\Delta\mathbf{R}^i$ (Rodriguez formula) can be found in References 3 and 9, e.g.

$$\Delta\mathbf{R}^i = \mathbf{1} + \frac{\sin\|\Delta\mathbf{w}^i\|}{\|\Delta\mathbf{w}^i\|}\Delta\boldsymbol{\Omega}^i + \frac{1}{2}\frac{\sin^2\|\frac{\Delta\mathbf{w}^i}{2}\|}{\|\frac{\Delta\mathbf{w}^i}{2}\|^2}(\Delta\boldsymbol{\Omega}^i)^2 \tag{24}$$

The construction of the discrete weak form is performed with the expressions given for $\Delta\mathbf{w}^i$, $\Delta\boldsymbol{\Omega}^i$ and $\mathbf{R}^i$. The following standard linearization process[3] of the discrete static weak form yields the tangent operator $\mathbf{K}^i$ and the residuum $\mathbf{G}^i$.

A POSTERIORI ERROR ESTIMATORS

It is the aim of this subject to discuss the validity of the linear 'error estimator' which is derived following Rheinboldt[4] and elaborated in detail by Verführt.[5] We mainly treat the following questions: 'Is it allowed only to consider the equilibrium and to take the residual forces into account but ignore the accuracy of the underlying metric in the non-linear continuum-mechanical stetting?' In order to clarify our answer 'yes and no', this section starts with reviewing Rheinboldt's justification of the use of an error estimator concerning the linearized problem. Then we discuss the conditions of this proof and treat two crucial situations namely bifurcation and locking phenomena which are of high importance in this paper. This section is concluded with some summarizing remarks and consequences from an engineering point of view.

Rheinboldt's derivation

We consider a real vector space $\mathbf{X}$ of displacement fields (a Banach space without loss of generality) with a norm $\|\cdot\|$ (e.g. energy norm) and a non-linear smooth mapping

$$\mathbf{G}:\mathbf{X}\mapsto\mathbf{X}^*$$

where the dual $\mathbf{X}^*$ represents the space of forces. For some load $\mathbf{p}\in\mathbf{X}^*$ and a scalar $\lambda\in\mathbb{R}$, the load factor, let $\lambda\cdot\mathbf{p}$, be the applied load which has to be in equilibrium with the reaction $\mathbf{G}(\mathbf{u})$ of the considered mechanical structure under the displacement field $\mathbf{u}\in\mathbf{X}$ (including boundary conditions),

$$\mathbf{G}(\mathbf{u}) = \lambda\cdot\mathbf{p} \tag{25}$$

Assume that $(\mathbf{u}_0, \lambda_0)$ satisfies (25), and $D\mathbf{G}(\mathbf{u}_0):\mathbf{X}\to\mathbf{X}^*$ is bijective, i.e. $D\mathbf{G}^{-1}(\mathbf{u}_0) =: \mathbf{K}(\mathbf{u}_0)^{-1}:$ $\mathbf{X}^*\to\mathbf{X}$ exists and is bounded. $D\mathbf{G}$ denotes (Frechet) derivative of $\mathbf{G}$. Then, the theorem on implicit functions shows (if $\mathbf{X}$ is a Banach-space) that there is some $\delta_1, \delta_2 > 0$ such that, for any λ with $|\lambda_0 - \lambda| < \delta_1$, there exists one and only one $\mathbf{u}\in\mathbf{X}$ with (25) and $\|\mathbf{u} - \mathbf{u}_0\| < \delta_2$, i.e. near $(\mathbf{u}_0, \lambda_0)$ we have a unique solution branch for (25). According to the inverse function theorem $D\mathbf{G}(u)^{-1}$ exists and is bounded near $\mathbf{u}_0$. Hence, without loss of generality, we may assume that

$$\|D\mathbf{G}(\mathbf{u})^{-1}\| \leqslant M_1, \quad \|D^2\mathbf{G}(\mathbf{u})\| \leqslant M_2$$

for any $\mathbf{u}\in\mathbf{X}$ with $\|\mathbf{u} - \mathbf{u}_0\| \leqslant \delta_2$ where $D^2\mathbf{G}$ is the second (Frechet) derivative of $\mathbf{G}$ assumed to be continuous. Since, in general, we cannot expect to know the solution $(\mathbf{u}_0, \lambda_0)$ exactly, we have to treat some approximation $(\tilde{\mathbf{u}}_0, \tilde{\lambda}_0)$ of it. In this approach the numerical treatment does not matter at this moment, it will be taken into account later in this section, but the approximation may be found computationally where $\tilde{\mathbf{u}}_0 = \mathbf{u}_h$ is the finite element solution.

The first assumption is that we have

$$|\lambda_0 - \tilde{\lambda}_0| \leqslant \delta_1 \quad \text{and} \quad \|\mathbf{u}_0 - \tilde{\mathbf{u}}_0\| \leqslant \delta_2$$

Due to the main theorem on calculus,

$$\begin{aligned}\mathbf{G}(\mathbf{y}) &= \mathbf{G}(\mathbf{x}) + \int_0^1 D\mathbf{G}(\mathbf{x} + t(\mathbf{y} - \mathbf{x}))[\mathbf{y} - \mathbf{x}]\,dt \\ &= \mathbf{G}(\mathbf{x}) + D\mathbf{G}(\mathbf{x})[\mathbf{y} - \mathbf{x}] \\ &\quad + \int_0^1 \int_0^t D^2\mathbf{G}(\mathbf{x} + s(\mathbf{y} - \mathbf{x}))[\mathbf{y} - \mathbf{x}][\mathbf{y} - \mathbf{x}]\,dt\end{aligned}$$

for any $\mathbf{x}, \mathbf{y} \in \mathbf{X}$ so that, for $\mathbf{y} = \mathbf{u}_0$ and $\mathbf{x} = \tilde{\mathbf{u}}_0$, it holds that

$$\|\mathbf{G}(\tilde{\mathbf{u}}_0) - \mathbf{G}(\mathbf{u}_0) - D\mathbf{G}(\tilde{\mathbf{u}}_0)[\mathbf{u}_0 - \tilde{\mathbf{u}}_0]\| \leqslant \frac{M_2}{2}\delta_2^2$$

Since $D\mathbf{G}(\tilde{\mathbf{u}}_0)$ is invertible with $\|D\mathbf{G}(\tilde{\mathbf{u}}_0)^{-1}\| \leqslant M_1$, we have

$$\|\mathbf{u}_0 - \tilde{\mathbf{u}}_0 - D\mathbf{G}(\tilde{\mathbf{u}}_0)^{-1}[\mathbf{G}(\tilde{\mathbf{u}}_0) - \mathbf{G}(\mathbf{u}_0)]\| \leqslant \tfrac{1}{2}M_1M_2\delta_2^2$$

Since $\mathbf{G}(\mathbf{u}_0) = \lambda_0 \cdot \mathbf{p}$, this yields

$$\|\mathbf{u}_0 - \tilde{\mathbf{u}}_0 + D\mathbf{G}(\tilde{\mathbf{u}}_0)^{-1}[\mathbf{G}(\tilde{\mathbf{u}}_0) - \lambda_0 \cdot \mathbf{p}]\| \leqslant \tfrac{1}{2}M_1M_2\delta_2^2 \tag{26}$$

Following Rheinboldt we consider the linearized equation evaluated at the known point $\tilde{\mathbf{u}}_0$, i.e. consider the solution $\mathbf{w}_0$ of the left-hand side of (26), namely

$$\mathbf{w}_0 = \tilde{\mathbf{u}}_0 - D\mathbf{G}(\tilde{\mathbf{u}}_0)^{-1}[\mathbf{G}(\tilde{\mathbf{u}}_0) - \lambda_0 \cdot \mathbf{p}]$$

Thus, $\mathbf{w}_0 \in \mathbf{X}$ solves the linear problem

$$D\mathbf{G}(\tilde{\mathbf{u}}_0)[\mathbf{w}_0 - \tilde{\mathbf{u}}_0] = \mathbf{G}(\tilde{\mathbf{u}}_0) - \lambda_0\mathbf{p} \tag{27}$$

Using the definition of $\mathbf{w}_0$, (26) gives

$$\|\mathbf{w}_0 - \mathbf{u}_0\| \leqslant \tfrac{1}{2}M_1M_2\delta_2^2 \tag{28}$$

which, using the triangle inequality twice, leads to the final result

$$\|\tilde{\mathbf{u}}_0 - \mathbf{u}_0\| \cdot (1 + c) = \|\tilde{\mathbf{u}}_0 - \mathbf{w}_0\| \tag{29}$$

where $|c| \leqslant (1/2)M_1M_2\delta_2$. Using Landau's symbol, this reads

$$\tilde{\mathbf{u}}_0 - \mathbf{u}_0 = (\tilde{\mathbf{u}}_0 - \mathbf{w}_0)(1 + O(M_1M_2\delta_2))$$

Conclusions

Using (29), Rheinboldt's argument is as follows: if δ_2 is small, which means that the approximation $\tilde{\mathbf{u}}_0$ is good, then, as seen in (29), the error $\|\tilde{\mathbf{u}}_0 - \mathbf{u}_0\|$ is nearly equal to the difference of the approximation and the solution of the linearized equation $\|\tilde{\mathbf{u}}_0 - \mathbf{w}_0\|$. Thus, it suffices to estimate the latter $\|\tilde{\mathbf{u}}_0 - \mathbf{w}_0\|$ dealing with a linear problem. Thus, the error indicators of the linear theory may be applied to the linear problem (27).

This conclusion is mathematically right and justifies the use of linear error indicators for an adaptive mesh refinement steering also in regular points of non-linear points. Hence, our answer about the justification of using linear error indicators is 'yes'.

This holds for an asymptotic behaviour when the constant c in (29) is small. For the above mentioned situation there exists some small number δ_2 such that the above justification is valid for all approximations $\tilde{\mathbf{u}}_0$ with $\|\tilde{\mathbf{u}}_0 - \mathbf{u}_0\| < \delta_2$. In practical situations it is not *a priori* clear that this holds. Therefore this must also be controlled within the iterative mesh refinement feedback algorithm.

Conversely, one main criticism is that the linear error indicator (i.e. the error indicator for the linearized problem (27)) deals with the residual, i.e. it treats only the forces but not the validity of the current configuration. In the mathematical analysis of the previous subsection, this is emphasized by the fact that δ_2 must be sufficiently small and hence that the (computed) approximation $\tilde{\mathbf{u}}_0$ must be sufficiently near to the exact solution $\mathbf{u}_0$. Moreover, the analysis turns out that asymptotically the influence of the wrong initial configuration (i.e. the influence of $\|\mathbf{u}_0 - \tilde{\mathbf{u}}_0\|$) on the error estimator is of 'one order lower' than the influence of the equilibrium (i.e. the influence of $\|\mathbf{G}(\tilde{\mathbf{u}}_0) - \lambda_0 \mathbf{p}\|$). But, again, this holds only in the sense of an asymptotic expansion, and may be false if $\|\mathbf{u}_0 - \tilde{\mathbf{u}}_0\|$ is not small enough.

In the following subsection we consider two examples of practical interest in which the use of the linearized error estimator is, in principle, not possible. In both cases, the constant M_1 is not bounded uniformly.

Robustness

As it is well-known, e.g. in the case of Reissner–Mindlin plates, the thickness t of the plate plays an essential role in the error analysis and leads to locking for $t \to 0$. The same phenomena can be observed in related shell models. Since the paper of Arnold (only 1-D), there are several mathematical contributions to the analysis of locking and which give several possibilities of stabilizing the numerical analysis. This gives robust methods leading to efficient approximations which overcome locking.

Mathematically, the essential observation is that (using an appropriate scaling) the thickness t appears partly in the tangent stiffness matrix as a factor $1/t^2$, i.e. the above constant M_2 depends on t, i.e.

$$M_1 = m_1, \quad M_2 = m_2 \frac{1}{t^2} \tag{30}$$

and m_1, m_2 do not depend on t. Note that, in this case, (28) gives

$$\|\mathbf{w}_0 - \mathbf{u}_0\| \leqslant m_1 m_2 \left(\frac{\delta_2}{t}\right)^2$$

such that we have to expect that the constant c in (29) is of order (δ_2/t).

In the next step we consider the finite element approximation. In the first example we assume that we have locking and are dealing with piecewise polynomials of degree p. Then, if h denotes the maximal element length in a quasi-uniform mesh (for simplicity), then the classical error estimate gives

$$\|\mathbf{u}_0 - \tilde{\mathbf{u}}_0\| \leqslant c \frac{h^p}{t^2}$$

i.e. linear convergence for piecewise linear elements and soforth, provided the thickness is constant. Assume that δ_2 may be equal to the left-hand side so that we may expect that

$$(\delta_2/t)^2 \approx \frac{h^{2p}}{t^4}$$

is the order of the constant c in (29). We remark that, in any shell or plate theory, usually, the thickness is not greater than the mesh size, even in adaptive methods. Therefore, $h^{2p}/t^4 \geqslant t^{4-2p}$. For linear elements and thin shells, this shows that the constant c in (29) may depend like c/t^2 which is far from being bounded. Thus, the use of the linear error indicators is useless in this case, our answer for the introduction's question is 'no'.

Note that the influence of locking is weakened if we use higher degrees of p.

In the second example we assume that we have some special elements without locking such we have some error estimate like

$$\| \mathbf{u}_0 - \tilde{\mathbf{u}}_0 \| \leqslant ch^p$$

i.e. linear convergence for piecewise linear elements and soforth, but a robust convergence, i.e. independent of thickness. Note that this concerns only the quality of $\tilde{\mathbf{u}}_0$ but not the fact that we have still (30). Hence, the above conclusions suggest that the constant c in (29) has the form

$$(\delta_2/t)^2 \approx \frac{h^{2p}}{t^2}$$

such that $p = 1$ leads to a reasonable use of the linearized error indicator.

Bifurcation

This paper treats stability problems in shell theory such that the use of the error indicator is of crucial importance and will be discussed in this subsection.

In the case of a stability point the tangent stiffness matrix becomes non-regular, hence the occurrence of the exceptional case can be observed numerically. Near the stability point the constant M_1 is high, and the constants δ_1, δ_2 are not greater than the distance of the point $(\mathbf{u}_0, \lambda_0)$ to the stability point $(\mathbf{u}^*, \lambda^*)$. Hence, it is not clear *a priori* that (i) $\| \mathbf{u}_0 - \tilde{\mathbf{u}}_0 \| < \delta_2$ since δ_2 is small and (ii) c is small because M_1 may be very large.

A more detailed analysis as in the first subsection shows that

$$\| \mathbf{G}(\tilde{\mathbf{u}}_0) - \lambda_0 \cdot \mathbf{p} - \mathbf{DG}(\mathbf{u}_0)[\mathbf{u}_0 - \mathbf{w}_0] \| \leqslant \frac{M_2}{2} \delta_2^2$$

is still valid. A closer look at the eigenvectors related to the smaller eigenvalues of $D\mathbf{G}(\mathbf{u}_0)$ shows that we have to decompose $\mathbf{u}_0, \tilde{\mathbf{u}}_0, \mathbf{w}_0$ in the direction of the crucial eigenvectors and the remaining part. Then, the above estimates (applied to the non-crucial directions) show that the estimate (29) holds in this case as well for the remaining, non-crucial part. Thus, up to the crucial directions the error indicators work well.

Summarizing, the linearized error indicators can be applied provided that the error of the approximation is good in comparison with the norm of the inverse of the tangential stiffness matrix and the second derivative of G. Otherwise, namely in case of locking or at bifurcation points, the linear error estimators may be useless for coarse finite element meshes.

Also bordering algorithms, e.g. the deflated decomposition of the solution near singular solution points,[10] cannot overcome this problem. This is shown in the sequal by investigating the linearization of (25) near singular equilibrium points $\mathbf{u}_o^*$ with the condition

$$\mathbf{G}(\mathbf{u}_h^*) - \mathbf{G}(\mathbf{u}_o^*) - \mathbf{DG}(\mathbf{u}_o^* - \mathbf{u}_h^*) = \mathbf{0} + \text{q.t.} \tag{31}$$

with $\mathbf{u}_o^* - \mathbf{u}_h^* =: \mathbf{e}^*$ and $\mathbf{G}(\mathbf{u}_h^*) - \mathbf{G}(\mathbf{u}_o^*) = \mathbf{R}^*$. By an appropriate shifting,

$$\mathbf{L}^* := \mathbf{DG}(\mathbf{u}_h^*) = \begin{bmatrix} \mathbf{L} & 0 \\ 0 & \varepsilon \end{bmatrix} \tag{32}$$

with $\|\mathbf{L}^{-1}\| \leqslant \nu_1$ and $\varepsilon \ll 1$, then multiplying (31) with the matrix $\begin{bmatrix} \mathbf{L}^{-1} & \mathbf{0} \\ \mathbf{0} & 1 \end{bmatrix}$ from the left-hand side and defining $\mathbf{e}^* := \begin{bmatrix} \mathbf{e}_1^* \\ e_2^* \end{bmatrix}$; $\mathbf{R}^* := \begin{bmatrix} \mathbf{R}_1^* \\ R_2^* \end{bmatrix}$, we get two equations, regarding the structure of $\mathbf{L}^*$, namely

$$\mathbf{L}^{-1}\mathbf{R}_1 = \mathbf{e}_1^* + \text{q.t.} \rightarrow \|\mathbf{e}_1^*\|^2 \leqslant \|\mathbf{L}^{-1}\| \cdot \|\mathbf{R}_1^*\| \tag{33}$$

with $\|\mathbf{L}^{-1}\| \leqslant \nu_1$ and

$$R_2^* = \varepsilon e_2^* + \text{q.t.} \rightarrow e_2^* = \frac{1}{\varepsilon} R_2^* + \frac{1}{\varepsilon} \cdot \text{q.t.} \tag{34}$$

such that the residuum cannot be reduced for growing dimension of $\mathbf{u}_h^*$ if ε is sufficiently small.[11]

This is especially important for branch switching into post-critical loading paths. The constant M_1 in (26) becomes large in this case but M_2 has still to be small. Outside of the ε surrounding, post-critical equilibrium points can be adaptively computed with the Rheinboldt indicators like pre-critical paths.

Implementation of Rheinboldts error indicator

Following non-linear load deflection curves within an iterative process, the displacement controlled Newton–Raphson method is not able to bypass points with vanishing $\det \mathbf{K}_T = 0$. But such extremals like limit points or bifurcation points are of great interest for structural engineers. The augmented system of non-linear equilibrium conditions for the arclength method overcomes the shortcomings by setting

$$\hat{\mathbf{G}}(\mathbf{v}, \lambda) = \begin{pmatrix} \mathbf{G}(\mathbf{v}, \lambda) \\ f(\mathbf{v}, \lambda) \end{pmatrix} = \mathbf{0} \tag{35}$$

where the non-linear function $f(\mathbf{v}, \lambda)$ describes the chosen arclength scheme. Linearization at an equilibrium point yields

$$\begin{pmatrix} \mathbf{G}_v & \mathbf{G}_\lambda \\ \mathbf{f}_v^T & f_\lambda \end{pmatrix} \begin{pmatrix} \Delta\mathbf{v} \\ \Delta\lambda \end{pmatrix} = -\begin{pmatrix} \mathbf{G} \\ f \end{pmatrix} \tag{36}$$

In order to obtain incremental stress states, the Frechet directional derivative yields

$$\Delta\boldsymbol{\sigma}_h = \frac{\partial \boldsymbol{\sigma}}{\partial \mathbf{v}} \Delta\mathbf{v}_{\text{trial}} = \mathbf{C}\mathbf{B}(\mathbf{v})\Delta\mathbf{v}_{\text{trial}} \tag{37}$$

where the different possible choices of $\mathbf{v}_{\text{trial}}$ are discussed in detail in the following chapter. Within a certain neighbourhood at bifurcation points measured with the norm $\|\mathbf{u}^* - \mathbf{u}^o\|$, the normalized eigenvector $\boldsymbol{\Phi}$ according to the lowest eigenvalue of $\mathbf{K}_T$ is used for applying the error estimator. The first eigenvalue may be very small but not zero. In this case we obtain the incremental displacement

$$\Delta\mathbf{v}_{\text{trial}} = \boldsymbol{\Phi}(\mathbf{K}_T(\mathbf{v}(\lambda_{\text{crit}}))) \tag{38}$$

where single valued bifurcations are assumed. Due to the results of this chapter, adaptivity is only possible before and after bifurcations.

The Babuška and Miller[12] error indicator is adequate for the linearized elastic problem, i.e. checking $\Delta\boldsymbol{\sigma}_h$. For bilinear shape functions only the projected stress jumps at element boundaries are usually relevant.

For a shell element i we get the *a posteriori* indicator with respect to its neighbours

$$\eta^2_{i\mathrm{MEM}} = \frac{t_i}{K^2_{i\mathrm{MEM}}} \int_{\partial\Omega_i} \mathbf{J}(\Delta\mathbf{n})^{\mathrm{T}}\,\mathbf{J}(\Delta\mathbf{n})\,\mathrm{d}s$$

$$\eta^2_{i\mathrm{BEN}} = \frac{t_i^3}{K^2_{i\mathrm{BEN}}} \int_{\partial\Omega_i} \mathbf{J}(\Delta\mathbf{m})^{\mathrm{T}}\,\mathbf{J}(\Delta\mathbf{m})\,\mathrm{d}s$$

$$\eta^2_{i\mathrm{SHEAR}} = \frac{t_i}{K^2_{i\mathrm{SHEAR}}} \int_{\partial\Omega_i} \mathbf{J}(\Delta\mathbf{q})^{\mathrm{T}}\,\mathbf{J}(\Delta\mathbf{q})\,\mathrm{d}s \tag{39}$$

$$\eta^2_{i\mathrm{BM}} = \eta^2_{i\mathrm{MEM}} + \eta^2_{i\mathrm{BEN}} + \eta^2_{i\mathrm{SHEAR}} \tag{40}$$

with

$$K_{\mathrm{BEN}} = \frac{Et_i^3}{12(1-\nu^2)}, \quad K_{\mathrm{MEM}} = \frac{Et_i}{1-\nu^2}, \quad K_{\mathrm{SHEAR}} = \kappa\frac{Et_i}{2(1+\nu)} \tag{41}$$

The heuristic Zienkiewicz and Zhu[13] error indicator does not yield an upper bound of the error in general, and the validity is dependent from the regularity of the real solution. Therefore convergence cannot be ensured. Furthermore, the proposed post-processing[14] might not yield superconvergence for strongly unstructured meshes due to the loss of accuracy within the blended interpolation. On the other hand this indicator can be easily computed and is used in this paper comparatively. Numerical experiments show that the Zienkiewicz and Zhu[13] indicator is effective for smooth solutions and polynomial degree $p = 1$.

A PRIORI INDICATORS

We have to decide between an indicator, concerning the model error of the problem, and a second one which controls the geometry of the adapted meshes.

Error of the non-linear model

It is obvious that the uniqueness of a solution cannot be guaranteed and only a local error analysis is possible.

An *a priori* error indicator restricts the relative rotations with respect to the limits of the applied theory, i.e. moderate, large or finite rotation shell theory. The incremental rotations should be $\leqslant 8°$ in the case of moderate rotation theory, e.g. As shown in References 1 and 15, instead of the complete material deformation gradient $\mathbf{F}_h(\mathbf{x}_h) = \mathbf{R}_h\mathbf{U}_h$ for deformations of the middle surface including initial curvatures, only the rotation can be controlled because $\mathbf{U}_h$ is near to the unity tensor for thin shells. $\mathbf{R}_h$ can be controlled by its linearization in the form

$$\tilde{\mathbf{R}}_h \cong \mathbf{1} + \boldsymbol{\Omega} = \begin{pmatrix} 1 & \omega_3 & -\omega_2 \\ -\omega_3 & 1 & \omega_1 \\ \omega_2 & -\omega_1 & 1 \end{pmatrix} \tag{42}$$

The indicator then follows as

$$\eta_{\mathrm{NL}} = \|\tilde{\mathbf{R}}_h - \mathbf{I}\|_2 = \max_{(\mathrm{nodes})}\sqrt{2(\omega_1^2 + \omega_2^2 + \omega_3^2)}. \tag{43}$$

η_{NL} is an absolute measure, e.g. $\eta_{\mathrm{NL}} \leqslant 0{\cdot}14$ for moderate rotation theory. According to this bound,

the incremental load factor has to be limited. We could also bind a norm of the incremental rotations $\Delta\boldsymbol{\beta}_\alpha$ directly.

Geometrically a priori indicators for mesh refining

Two strategies of the *h*-method for plates and shells are realized

(1) regular refinements of quadrangles with irregular (hanging) nodes and
(2) irregular element refinement saving regular nodes.

The latter is preferable in the case of non-linear theories because interpolations for irregular nodes are rather complicated. Nested approximation spaces with halvened element lengths are used. This is advantageous for multigrid method and other multilevel solution methods. The usual limitation for length ratio, scewness, aspect ratio and taper are regarded in the mesh generator.

DESCRIPTION OF THE REFINEMENT STRATEGY FOR GEOMETRICALLY NON-LINEAR PROBLEMS

In order to derive a suitable refinement strategy for geometrically non-linear problems we have to distinguish between two different kinds of problems. There are a lot of slightly modified possibilities to obtain a refinement criterion in both cases.

Following a geometrically non-linear load displacement pattern, the question of appropriate stresses for computing the error indicators arises. The Frechet directional derivative (35) might be used in order to compute a suitable stress increment for the application of a stress-based indicator.[12] But the derivative can be evaluated into various directions. First of all, we may choose the difference of displacements between two neighbouring configurations on the equilibrium path. This strategy is prefered in this paper in very good agreement with the mathematical preliminaries of the section on *a posteriori* error estimates, and it is always applied without any numerical problems. Another possibility arises by using the first step of a Newton–Raphson iteration.

From the computational point of view the computation of a Frechet directional derivative needs special efforts. We have to take care of special features for every finite element formulation, and the computer code has to be changed for every new element. Therefore it seems to be much easier to calculate the stresses of two neighbouring configurations on the equlibrium path. The differences between these stress states result in an allowable stress increment for adaptation. Finally the direct application of the whole stress state for evaluating the stress indicators gives in some cases good results too.

The self-adaptive computation of bifurcation points needs an iterative strategy. We start with a coarse finite element mesh and try to detect the bifurcation point with a path following method, i.e. controlling the number of negative diagonal elements and the determinant. This method allows to find the single valued bifurcation point of interest.

Then the normalized eigenvector is used in order to get a stress increment for computing the refinement criterion and for branch switching too. As mentioned above, different methods of getting a stress increment are possible, and this holds for the special case of bifurcation problems too. But the application of the Frechet derivative in the direction of the normalized eigenvector has proved to be the most effective one which results in the best-fitted meshes for analysing bifurcation problems.

Following secondary paths after branch switching the actual displacement increment is used to construct a new stress increment for further adaptive refinement.

ASPECTS OF DIMENSIONAL ADAPTIVITY IN DISTURBED 2-D SUBDOMAINS

Introduction and concepts

Modeling of thin-walled beams, plates and shells as 1-D and 2-D BVP's due to kinematical hypothesis, e.g. the normal hypotheses, is valid in undisturbed domains. Disturbances near supports and free edges, in the vicinity of concentrated loads and at thickness jumps cannot be described by 1-D and 2-D BVP's. In these disturbed subdomains, dimensional adaptivity has to be performed with respect to the 3-D theory. Dimensional adaptivity (*d* adaptivity) coupled with an *h* or *p* adaptivity becomes necessary in oder to guarantee a reliable overall solution.

The two different ways of realization are the 'Reduction Model' (RM) and the 'Expansion Model' (EM). RM starts from the 3-D model, checking the hypotheses of the 2-D model,[16–18] within undisturbed subdomains (Table I (2b)). It is the proper mathematical way and can include different stages between the simple 2-D theory and the complete spatial formulation. A disadvantage is the need for *a priori* 3-D computations and the necessity of advanced elements, e.g. with the

Table I. Strategies for h–p–p_t–d adaptive finite-element methods solving 2-D BVP's with 3-D disturbances

Expansion method	Reduction method
(1a) h–d adaptivity Startmesh 2-D displacement plate elements h-adaptivity heuristic estimator 2-D → 3-D elements	(2a) h–d adaptivity Startmesh 3-D order of elements higher than Q1 h-adaptivity proper estimator 3-D → 2-D elements
Advantages Small startmesh, main computations in 2-D domain	*Advantages* Estimator from error analysis with upper bounds
Disadvantages Heuristic indicator for d-adaptivity → Controlling error rates in 2-D and decay lengths according to St. Venant's principle	*Disadvantages* Big 3-D startmesh reduction of meshes
(1b) h–p_t–d adaptivity Startmesh 2-D higher order h–p_t elements h–p_t adaptivity heuristic estimator 2-D → 3-D elements	(2b) hp–p_t–d adaptivity Startmesh 3-D anisotropic h_p volume elements h_p–p_t–d adaptivity estimator from error-analysis 3-D → 2-D elements
Advantages Small startmesh, main computations in 2-D domain improved convergence relative to (1a)	*Advantages* Asymptotic and improved convergence relative to (2a) smaller startmesh than (2a)
Disadvantages Heuristic indicator for d-adaptivity → controlling error rates $2\frac{1}{2}$D and decay lengths according to St. Venant's principle	*Disadvantages* Relatively big system of equations complicated mesh reduction

p_t version in thickness direction (multilevel hierachical p_t–ph–d anisotropic elements). If the p or p_t algorithm is not included, h–d adaptivity is obtained (Table I (2a)). This method is not so effective as the h–p_t–d adaptivity (Table I (2b)).

EM starts from the 2-D model, changing to the 3-D model within disturbed subdomains using heuristic *a priori* indicators (e.g. decay length of singularities) and *a posteriori* indicators of the 2-D and 3-D model (Table I (1a)). This method is more effective if anisotropic h–p_t elements are invoked (h–p_t–d adaptivity Table I (1b)). Furthermore, EM is favourable in case of changing thickness and especially haunched plates, e.g. near columns, because hierarchical RM models become theoretically complicated in these cases.

In Table I the advantages and disadvantages of these different models are summarized. In this paper, we want to discuss EM (Table I (1a)).

Additionally, our recent papers[1,15,19] have been concerned with problems arising in the RM strategy. Remark: Due to recent results, the heuristic estimation in EM is replaced by a proper error-estimator, when the estimators in (46), (47) are calculated from the 3D-system and boundary conditions and if we furthermore add to (46), (47) the residuals in the element domains within the 3D setting. Then the EM error estimators are proper ones like in RM.

Concept of the d–h adaptivity with the expansion method

The basic concept of the combined multileveled h–d adaptivity procedure consists of stepwise checks of h adaptivity, of the St. Venant's principle applied to the 3-D elasticity problem and finally of the local error-evolution for 2-D indicators within the h-refinement. These are three main steps of criteria for transition from h adaptivity to d–h adaptivity all of which have to become active for d adaptivity.
These indicators are as follows.

Indicator: value of the local error indicator. The first check is the value of the local element error indicator (η_e) in the 2-D domain. The Babuška and Miller[12] error indicator is used neglecting the residua within the element domains, i.e. restricting ourselves so far to the projected stress jumps at the element boundaries which is an approximation already for Q1 elements. Meanwhile, the complete residual error indicator has been implemented into the codes, i.e. even residua in the element domains.

$\mathbf{t}_h^+; \mathbf{t}_h^-$: stress vectors at both sides of an element interface according to

$$\text{Cauchy's theorem} \rightarrow \mathbf{t}^+ = -\mathbf{t}^- \tag{44}$$

$\mathbf{J}(\mathbf{t}_h)$ is the jump of the approximated stress vector, where $+$ denotes the section with positive co-ordinate increments

$$\mathbf{J}(\mathbf{t}_h) = \mathbf{t}_h^+ - \mathbf{t}_h^- \tag{45}$$

In this context the local Babuška–Miller[12] indicator is used in the following version for the h–d adaptivity

$$\eta_e^2 = \frac{1}{2} ch \int_{\partial\Omega_e} \mathbf{J}_e(\mathbf{t}_h)^t \mathbf{J}_e(\mathbf{t}_h)\, dA \tag{46}$$

which yields the resulting global error indicator

$$\eta_G^2 = \frac{1}{2} c \sum_e h_e \int_{\partial\Omega_e} \mathbf{J}_e(\mathbf{t}_h)^t \mathbf{J}_e(\mathbf{t}_h)\, dA. \tag{47}$$

In order to control dimensional adaptivity near edges we introduce the stress jumps at the system

boundaries (supported as well as free edges),

$$\mathbf{J}(\mathbf{t}_h)_{\text{system boundary}} = \mathbf{t}_h^+ \tag{48}$$

If this error reaches a tolerance η_{krit}, the indicators 2 and 3 must be checked. For $\eta_e < \eta_{\text{krit}}$ mesh refining is automatically stopped at this element. Summarizing, the local error indicator has to be larger than the tolerance $\eta_{\text{krit.}}$ in order to check d adaptivity in the next step.

Indicator: decay length of the local 2-D error from 3-D elasticity according to St. Venant's principle. For plates and shells, the decay length is (2–3)t according to St. Venant's principle (with t being the thickness of the structure), dependent on the type of the singularity, e.g. $\ln(r)$ or $1/r$. If the local element size is bigger than $h_{\text{krit}} = 2{\cdot}5t$, then h adaptivity of the 2-D problem is applied. If the local element size is smaller than h_{krit} then the third indicator must be checked.

Indicator: local error rate. At each refinement step of 2-D h adaptivity, the local error rate θ_e is computed from two successive meshes.

Refining mesh i into mesh $i + 1$, the evolution of the local error $\eta^2_{e_{(i)}} \to \eta^2_{e_{(i+1)}}$ defines the error rate as

$$\theta_{(i+1)} = \theta_{(i)\to(i+1)} := \frac{\eta^2_{e_{(i+1)}}}{\eta^2_{e_{(i)}}} \tag{49}$$

The element $e_{(i+1)}$ is a daughter element of element $e_{(i)}$. The element area of $e_{(i+1)}$ is a quarter of the element $e_{(i)}$ (Figure 2).

For Q1 elements with sufficient regularity of the solution, the error rates are

$$\begin{aligned} &\theta \approx 1/16 \quad \text{for normal improvement} \\ &\theta \approx 1/4 \quad \text{for less improvement} \\ &\theta \approx 1/2 \quad \text{in case off deterioration} \end{aligned} \tag{50}$$

In the following example of a hypar shell the critical error rate is chosen as $\theta_{\text{krit}} = \sqrt{1/32}$. If the local error rate is bigger than θ_{krit} and the indicators 1 and 2 are activated, then the dimensional jump is realized regarding also *a priori* criteria for mesh generation. If the local error rate is smaller than the critical error rate and the indicators 1 and 2 are activated, then only h adaptivity in the 2-D subdomain is applied. Figure 3 shows the scheme of conditions for h–d adaptivity.

Aspects of mesh generation, mainly the transition from 2-D to 3-D domains

The 3-D domain is connected with the 2-D domain with the help of kinematic transition elements. They are automatically generated when we switch from a 2-D element to a 3-D element. Transition elements generated at the same spatial position, e.g. transition between domains with

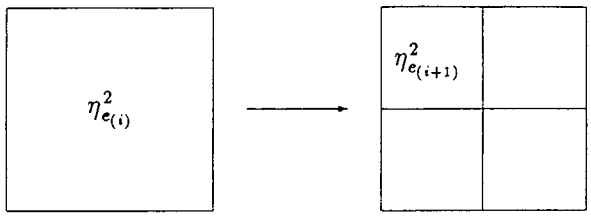

Figure 2. Development of the error from element $e_{(i)}$ to some daughter element $e_{(i+1)}$, see equation (49)

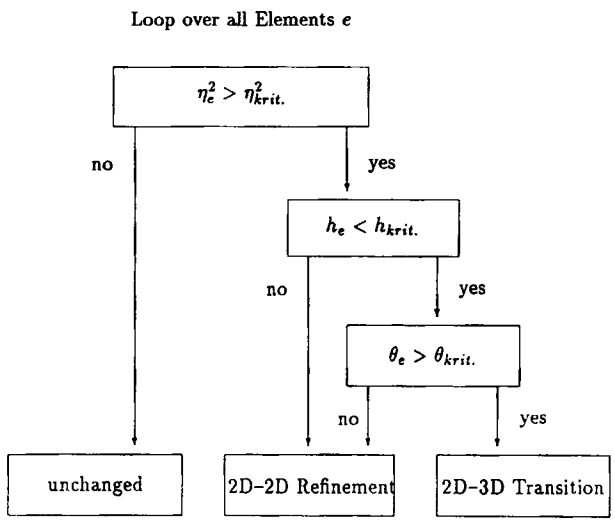

Figure 3. Scheme of h–d criteria for 2-D refinement and 3-D transition in the expansion method of dimensional adaptivity

the same dimension, are subsequently deleted (according to the rule: identical transition elements are deleted).

The first error indicators (Babuška–Miller indicator η_e) of 2-D and 3-D elements are computed in the same way. The stresses at transition from 2-D to 3-D meshes are determined by using virtual 3-D elements for the 2-D modelling. Therefore, the computation of error indicators for the h–d adaption follows the same lines as for the h adaption in 3-D domains.

Remarks on the robustness and validity of the expansion method

Due to the fact that the three indicators η_{krit}, h_{krit} and θ_{krit} have to become active together the incremental and iterative process of d adaptivity showed up to be insensitive and stable with respect to changes of the start meshes and to the reasonable choice of tolerances for η_{krit}, h_{krit} and θ_{krit}. The boundary conditions are controlled for the 3-D system such that boundary layers must show up. It is notable that the engineering insight into the results of the refinement process and the computational asymptotics of displacements and stresses permit a direct control of the reliability.

Yet it has to be remarked that the error estimation of the 3-D model is principally not possible completely by checking the error rate with low p order h refinements within the 2-D plate model. By power expansions of the model error using orthogonal functions it can turn out that higher p modes are important in the layer zones. Then p_j adaptivity is necessarily controlled by anisotropic error estimators in the directions x_j, $j = 1, 2, 3$, especially in the normal direction x_3 (p_t adaptivity)), see Table I and References 16–18.

Several strategies are possible to overcome this within a mixed expansion–reduction method, namely,

(i) checking the energy for higher p modes on element patches in order to select the dominant ones or
(ii) checking the local convergence rates for h refinement and enlarge p if the rates θ_j (see equation (49)) are larger than θ_{krit}, i.e. if the local regularity of the solution is high enough.

The general goal is to balance reliability and effectivity by improving the solution and the model in a staggered, so to say 'diagonal' procedure. Of course the solution error must be always smaller than the model error. Further research using different levels of degenerated shell elements and 3-D elements is in progress. Finally it should be mentioned that different philosophies of thinking are usual in engineering and mathematics. Engineers like to develop their models in a growing complexity (expansion) whereas mathematicians use deductive procedures from general to less complex models (reduction).

EXAMPLES

In this section we present three examples illustrating the effectiveness of the present refinement strategies. For h–d adaptivity, an infinite field of edge-supported hypar shells is investigated by one member of this field in the framework of the geometrically linear theory. The solution is compared with results obtained from a pure 2-D non-linear shell analysis. Adaptive computations of both problems allow a comparison between geometrical linear and non-linear theory and shows especially the influence of d adaptivity at the supports.

Next, we treat the post-buckling analysis (branch switching) of a simply supported cylinder. Adaptive meshes for the secondary equilibrium path give a deeper understanding of the buckling modes and the failure of these structures for practical engineering problems.

Example for dimensional adaptivity

Figure 4 shows the infinite hypar shell system. At the points denoted by the small circles the shells are supported (fixed in z direction at the bottom surface). Four shells with uniform loads are

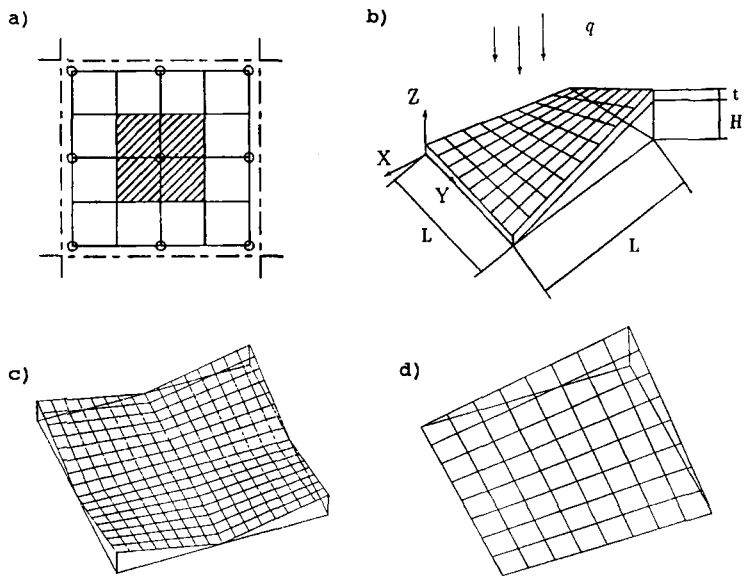

Figure 4. System of four continuous hypar shells supported at the lower centre points, $L = 10$ m, $t = 0{\cdot}2$ m, $H = 2{\cdot}5$ m, $q = -5 \times 10^3$ Nm^{-2}, E $= 1{\cdot}0 \times 10^8$ kNm^{-2}, $\nu = 0$, width of the support $b = 0{\cdot}625$ m $= (1/32)L$. The system has symmetry conditions at each side and it is fixed on a simple column (a) system, (b) system data, (c) system with start mesh and a quarter of the system (d) start mesh for a quarter of the system

depicted in Figure 4(c). In Figure 4(b) the system datas are given, and Figure 4(d) shows the starting mesh.

In Figure 5 the deformed mesh (with enlarged deformation) is shown with a 3-D discretized subdomain in the vicinity of the support. This result is calculated within the 6th step of h–d adaptivity. Figure 6 shows the zoomed supported area in order to obtain a more close view on

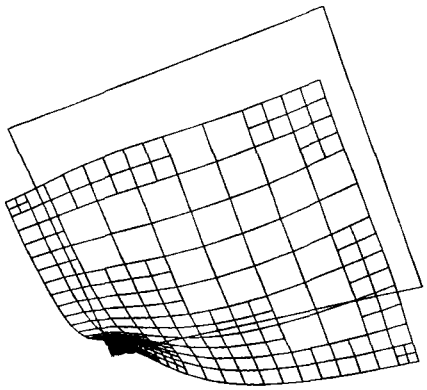

Figure 5. Deformed mesh, scaled deformation with 6. step of h–d adaptivity

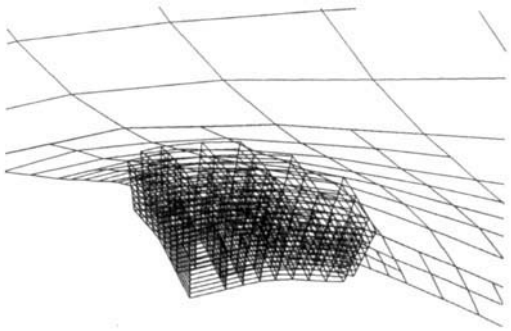

Figure 6. Deformed mesh, scaled deformation, with 6. step of h–d adaptivity, zoomed in the vicinity of the support

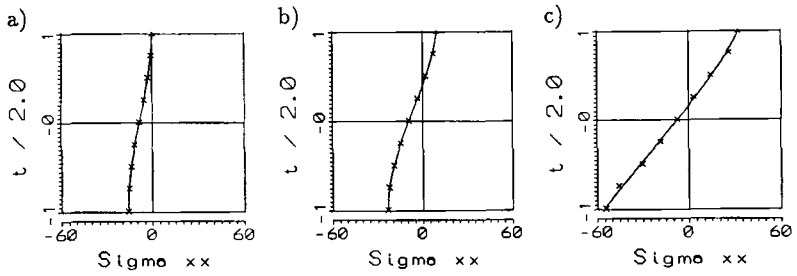

Figure 7. Results of σ_{xx} (MPa) at the points (a) $x = 0{\cdot}0$ m, $y = 0{\cdot}3215$ m, (b) $x = 0{\cdot}3125$, $y = 0{\cdot}3125$ m, (c) $x = 0{\cdot}625$ m, $y = 0{\cdot}3125$ m in Figure 4(b). The points (a) and (b) are at the support, the point (c) is close to the support

the 3-D domain. The σ_{xx} stresses near the support are presented in Figure 7. It is obvious that the kinematic hypothesis of the shell theory is not valid.

In Figure 8 the error development with increasing number of d.o.f.'s (equations) is shown. Above 3588 d.o.f.'s the curve has a kink due to the activation of the dimensional jump. Q1 and Q2 elements are applied in the 3-D domain.

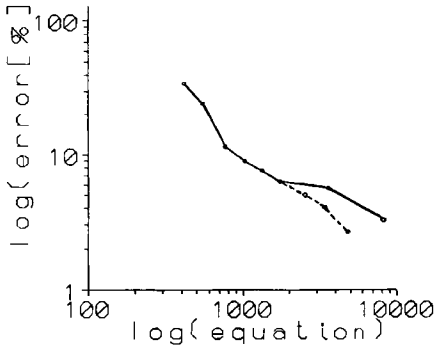

Figure 8. Relative global error in the energy norm depending from the number of unknowns in douple-logarithmic scale, including the influence of d adaptivity. (——), Q1 elements in 3-D; (– – – –), Q2 elements in 3-D

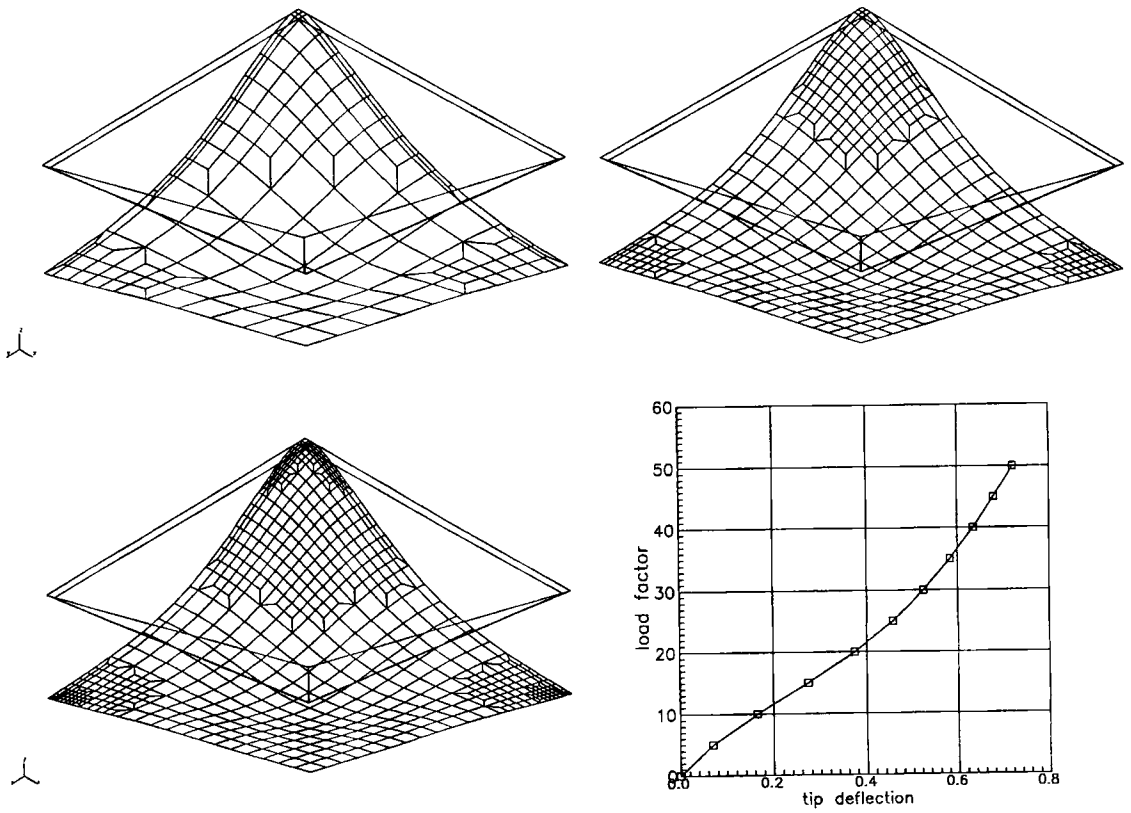

Figure 9. Hyperbolic shell, geometrically non-linear analysis for an equally distributed vertical load $p = \lambda P_{ref}$, $P_{ref} = -5{\cdot}0\,\mathrm{kNm}^{-2}$, (a)–(c) deformed adaptive meshes, (1086, 2682, 4092 d.o.f.), d vertical displacement U_z of point A

Hyperbolic shell

The hyperbolic shell in Figure 4 is investigated where Figure 9 shows the birds eye view of adaptive meshes and the deformed shell with a zooming factor of 5·0. The three successive refinements shown hold for a tip deflection of (1/3) H. The different meshes in comparison with Figure 5 result from geometrically linear vs. non-linear analysis.

Adaptive post-buckling analysis of an axially loaded cylinder

The buckling analysis of cylinders is of great importance for structural engineers, and there are many publications devoted to this subject. Figure 10 shows an axially loaded cylinder with

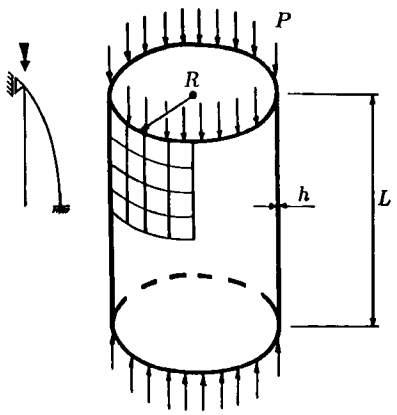

Figure 10. Cylindrical shell, geometry and loading $R = 100\,\text{m}$, $L = 140\,\text{m}$, $h = 2\,\text{m}$, $E = 30 \cdot 10^3 \text{kNm}^{-2}$, $\nu = 0$, $P = \lambda P_{\text{ref}}$, $P_{\text{ref}} = 693{\cdot}2\text{kNm}^{-1}$ and start mesh in the eighth of shell

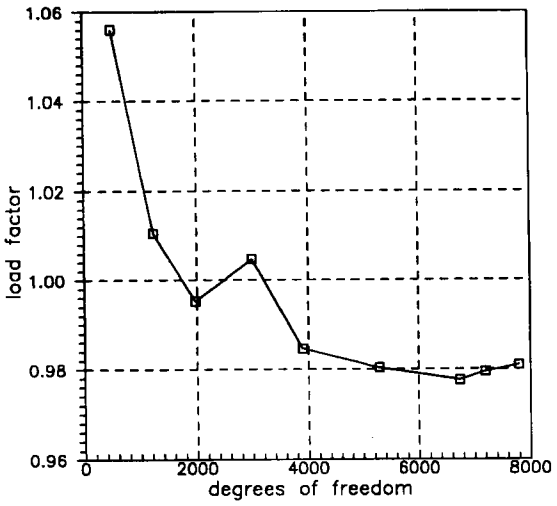

Figure 11. Convergence properties of the adapted meshes with respect to the critical load of cylinder Figure 10

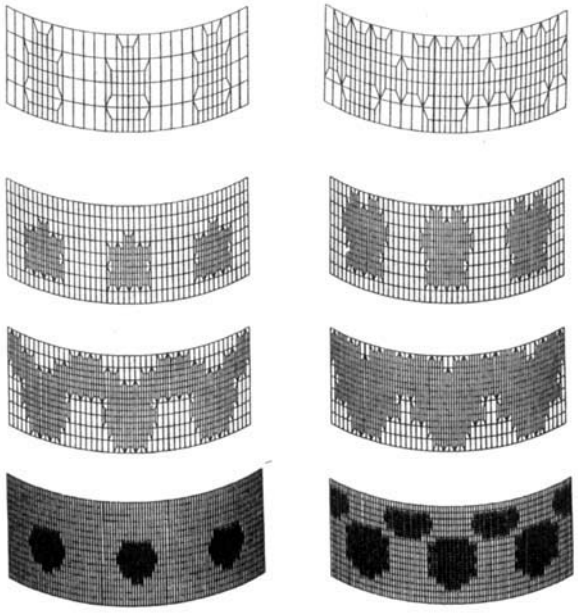

Figure 12. (a)–(h) Sequence of nested adapted meshes for the cylindrical shell, (1011, 1431, 3205, 4135, 5187, 6165, 10 791, 15 100 d.o.f.)

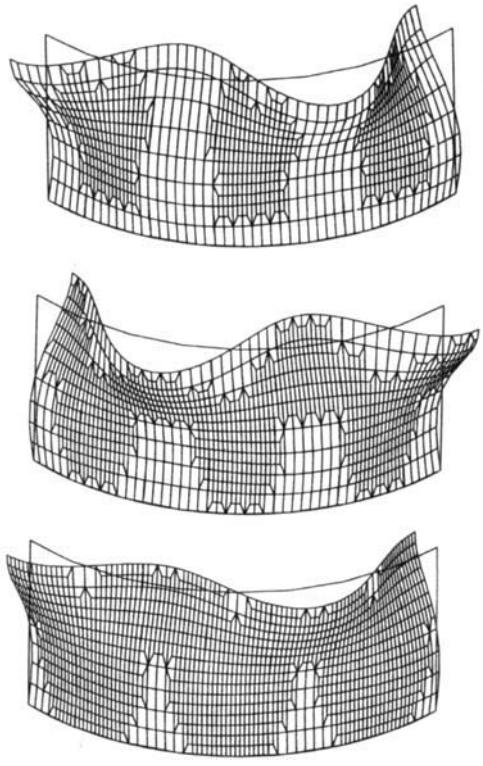

Figure 13. Branch switching mode (4135, 5187, 6165 d.o.f.) approximated by a sequence of mesh refinements

vanishing lateral displacements on both edges. A quarter in the circumferential direction and one half of the length are considered. Only even-numbered deformation patterns in both directions are admitted. The lowest bifurcation load λ_{krit} cannot be obtained by this restricted modelling, and therefore the whole system has to be investigated in general. The advantages of the presented adaptive concept are very striking. In this example six waves are expected in the circumferential direction and one wave over the length.

The calculation is performed with the finite element formulation presented in section on introduction of this paper. As the underlying theory allows finite rotations it is very suitable for detecting secondary paths into deep post-buckling branches.

Figure 11 displays the development of the calculated lowest bifurcation load for different types of adapted meshes. It is remarkable to note that the load factor does not change any more when the number of degrees of freedom has reached nearly 5000 unknowns which correspond to the third adapted mesh. Between the second and the third uniquely refined mesh there are still changes, and the numerical effort ($O(n^2)$) to get results for the third uniquely refined mesh (7800 d.o.f.'s) has to be compared with the automatic feedback analysis (max. 5000 d.o.f.'s) which shows its effectivity.

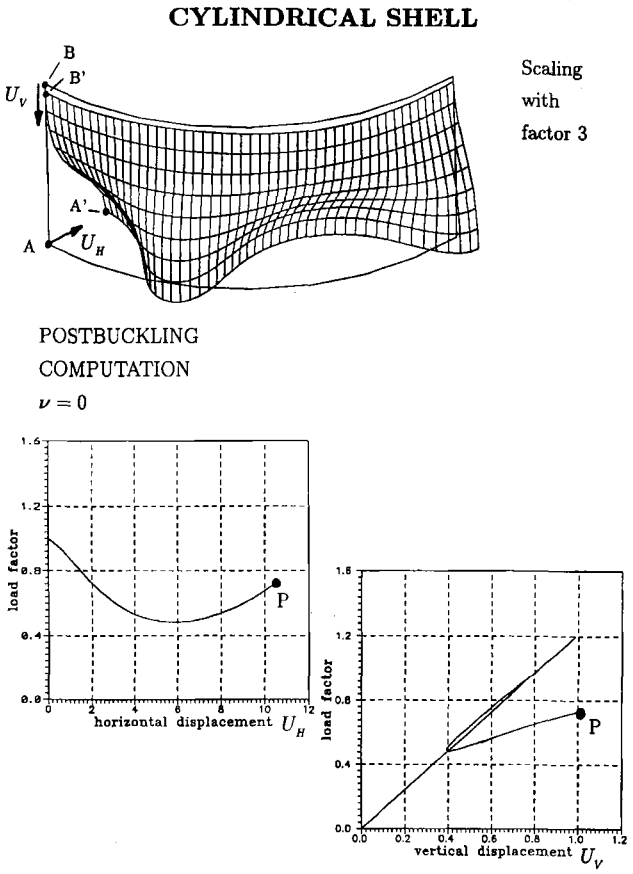

Figure 14. Adaptive computation of postbuckling equilibrium point P for cylindrical shell from Figure 10. (a) startmesh and scaled deformation of an upper eighth of the cylinder, (b) horizontal displacement of point A, (c) vertical displacement of point B

Figures 12 (a–f) show how the refined zones spread out in the adapted meshes where the error indicators are evaluated close to the bifurcation point. Figures 12(g) and (h) show higher levels of mesh adaptation. Figures 13(a–c) display a series of refined meshes near the bifurcation point, Figures 12 (d–f), using the scaled branched eigenmode.

The post-critical analysis of the cylinder with the starting mesh is given in Figures 14(a–c). Figure 14(a) shows the deformed start mesh at point P (see Figures 14(b) and (c)) of the

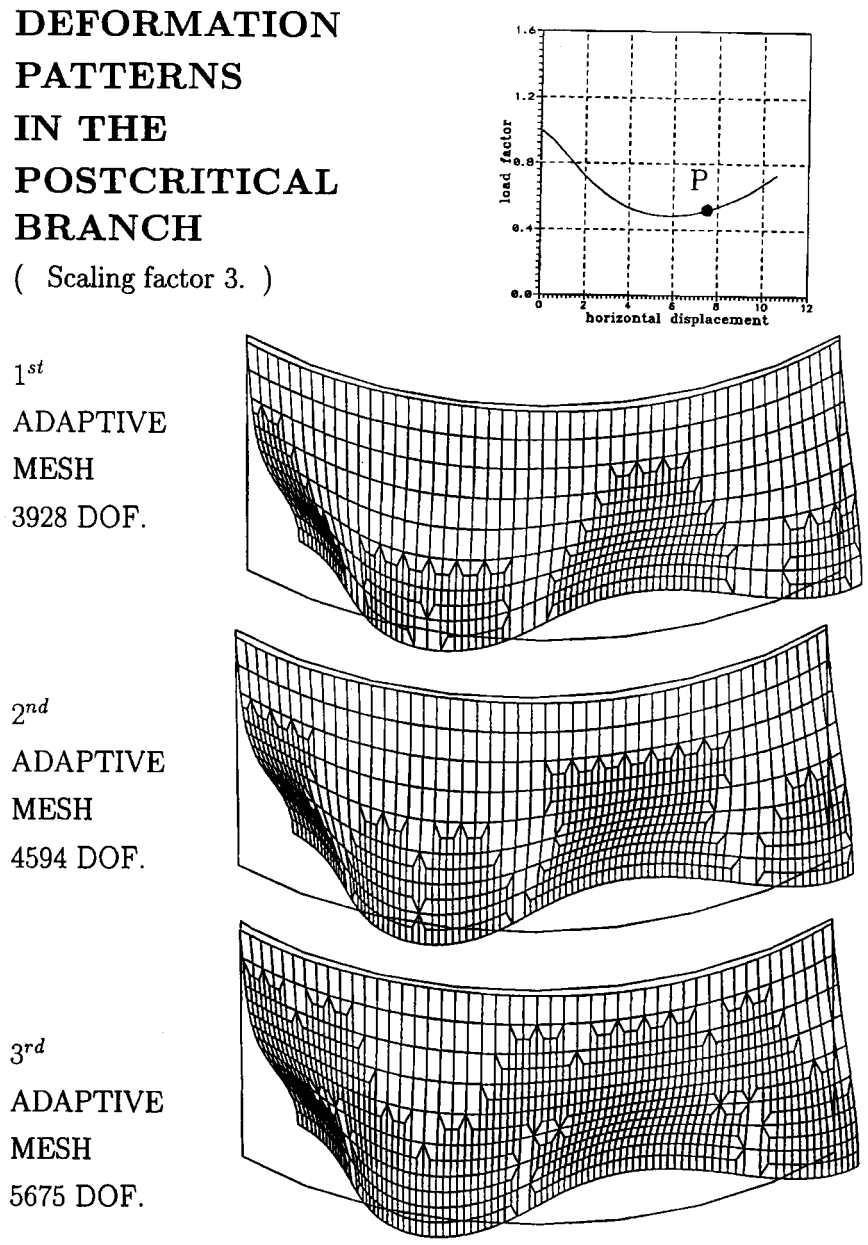

Figure 15. (a)–(d) Sequence of nested adaptive meshes for post-critical equilibrium point P in (a)

post-critical solution branch. The resulting first, second and third adaptive meshes for further analysis of the post-critical branch are displayed in Figure 15.

CONCLUSIONS

An advanced refinement strategy is presented for geometrically non-linear problems. This strategy includes a shell element for finite rotations within the frame of Reissner–Mindlin kinematics and an error analysis for these shell problems. The known concept of adaptivity is theoretically expanded in order to get deeper insight into bifurcation problems and related questions. One main result of this paper is that the used concept of adaptivity is not possible directly at bifurcation points (because of non-unique solutions) and that asymptotic convergence cannot be obtained for locking dominated problems. What is evident is that the robustness of the chosen mechanical and numerical model has to be investigated separately.

The whole strategy is completed by the dimensional adaptivity which allows a consistent and stable modelling and an iterative procedure for non-linear load–deflection curves and branch switching. The computer code was developed within our system INA-SP; it is a flexible tool for a rather general class of non-linear problems.

REFERENCES

1. E. Stein, W. Rust and S. Ohnimus, '*h*- and *d*-adaptive FE element methods for two dimensional structural problems including post-buckling of shells', in *Proc. the 2nd Workshop on Reliability in Computational Mechanics*, Krakov, 1991; *Comput. Methods Appl. Mech. Eng.*, **101**, 315–354 (1992).
2. F. Gruttmann, E. Stein and P. Wriggers, 'Theory and numerics of thin elastic shells with finite rotations', *Ing. Archiv.* **59**, 54–67 (1989).
3. J. C. Simo, D. D. Fox and M. S. Rifai, 'On a stress resultant geometrically exact shell model, Part III: computational aspects of the nonlinear theory', *Comput. Methods Appl. Mech. Eng.*, **79**, 21–70 (1990).
4. W. C. Rheinboldt, 'Error estimates for nonlinear finite element computations', *Comput. Struct.*, **20**, 91–98 (1985).
5. R. Verfürth, 'A posteriori error estimation and adaptive mesh-refinement techniques', *J. Comp. Appl. Math.* (to appear).
6. E. N. Dvorkin and K. J. Bathe, 'A continuum mechanics based four node shell element, for general nonlinear analysis', *Eng. Comput.* **1**, 77–88 (1984).
7. P. Wriggers and F. Gruttmann, 'Thin Shells with Finite Rotations Formulated in Biot Stresses: Theory and Finite Element Formulation', *Int. j. numer. methods eng.*, **36**, 2049–2071 (1993).
8. F. Gruttmann, W. Wagner and P. Wriggers, 'A nonlinear quadrilateral shell element with drilling degrees of freedom', *Arch. Appl. Mech. (Ing. Archiv.)* **62**, 474–486 (1992).
9. J. H. Argyris, 'An excursion into large rotations', *Comput. Methods Appl. Mech. Eng.*, **32**, 88–155 (1982).
10. T. F. Chan, 'Deflated decomposition of solutions of nearly singular systems', *SIAM J. Numer. Anal.*, **21**, 738–754 (1984).
11. R. Verfürth, 'A posteriori error estimates for non-linear problems. Finite element discretizations of elliptic equations', *Math. Comput.* (1994) in press.
12. I. Babuška and A. Miller, 'A feedback finite element method with a posteriori error estimates: Part I. The finite element method and some properties of the a posteriori estimator', *Comput. Methods Appl. Mech. Eng.*, **61**, 1–40 (1987).
13. O. C. Zienkiewicz and J. Z. Zhu, 'A simple error estimator and adaptive procedure for practical engineering analysis', *Int. j. numer. methods eng.*, **24**, 337–357 (1987).
14. N.-E. Wiberg and F. Abdulwahab, 'An efficient postprocessing technique for stress problems based on superconvergent derivatives and equilibrium', in Proc. *First European Conference on Numerical Methods in Engineering* (7–11 Sept. 1992), *Int. j. numer. methods eng.*, 25–32 (1992).
15. E. Stein and S. Ohnimus, 'Concept and realisation of integrated adaptive finite element methods in solid- and structural-mechanics', in *Proc. 1st European Conf. on Numerical Methods in Engineering* 7–11 September 1992, Brussels, Belgium; *Int. j. numer. methods. eng.*, 163–170 (1992).
16. S. Jensen and I. Babuška, 'Dimensional reduction for nonlinear boundary value problems', *SIAM J. Numer. Anal.*, **25**, 644–669 (1988).
17. S. Jensen, 'Computational aspect of adaptive dimensional reduction for nonlinear boundary value problems', In J. Robinson (ed.), *Finite Element Methods in the Design Process*, Robinson and Associates; Okehampton; UK, 1990.
18. S. Jensen, 'Adaptive dimensional reduction for scalar boundary value problems, Department of Mathematics', University of Maryland, Baltimore, 1991.

19. E. Stein and S. Ohnimus, Dimensions-Adaptivität bei Finite-Element-Berechnungen von Stäben und Platten, ZAMM **73**, 6 (1993).
20. I. Babuška and W. C. Rheinbol, 'Error estimates for adaptive finite element computations', *SIAM J. Numer. Anal.*, **15**, 736–754 (1978).
21. E. Stein, W. Wagner and P. Wriggers, 'Concepts of Modelling and Discretization of Elastic Shells for Nonlinear Finite-Element Analysis', in *The Mathematics of Finite Elements and Application*, MAFELEAP 1987, pp. 205–232 (1988).
22. E. Stein and W. Rust, 'Mesh adaptations for linear 2D finite element discretizations in structural mechanics, especially in thin shell analysis', *J. Comput. Appl. Math.*, **36**, 107–129 (1991).